Supporting Information for

Development and Modification of Porous Polymer Structures in the Vicinity of Cellulose Fibers

Sebastian Pusse[1], Sebastian Heinz[1], Waranya Limprasart[2], Lea Gemmer[1], Suteera Witayakran[1,4], Samuel Schabel[3], Volker Presser[5,6,7], Torsten Gutmann[2,8] and Markus Gallei[1,7*]*

[1]Polymer Chemistry, Saarland University, Campus C4 2, 66123 Saarbrücken, Germany

[2] Eduart-Zintl-Institute for Inorg. and Phys. Chemistry, Technical University Darmstadt, Peter-Grünberg-Straße 8, 64287 Darmstadt, Germany[3] Mechanical Engineering, Chair of Paper Technology and Mechanical Process Engineering, Technical University of Darmstadt, Alexanderstraße 8, Darmstadt, 64283, Germany

[4] Max Planck Institute for Informatics, Saarland Informatics Campus, E1 4, 66123 Saarbrücken, Germany 66123, Germany

[5] INM - Leibniz Institute for New Materials, Saarbrücken 66123, Germany;

[6]Department of Materials Science and Engineering, Saarland University, Campus D2 2, Saarbrücken 66123, Germany

[7] Saarene, Saarland Center for Energy Materials and Sustainability, Saarland University, Campus C4 2, 66123 Saarbrücken, Germany

[8] Department of Chemistry, Physical Chemistry, University of Paderborn, Warburger Straße 100, 33098 Paderborn, Germany

Corresponding Authors:

*Markus Gallei: markus.gallei@uni-saarland.de

*Torsten Gutmann: gutmann@chemie.tu-darmstadt.de

$$x(A) = \frac{\left(\frac{I(A)}{N(A)}\right)}{\left(\frac{I(A)}{N(A)}\right) + \left(\frac{I(B)}{N(B)}\right)} \qquad \text{S1}$$

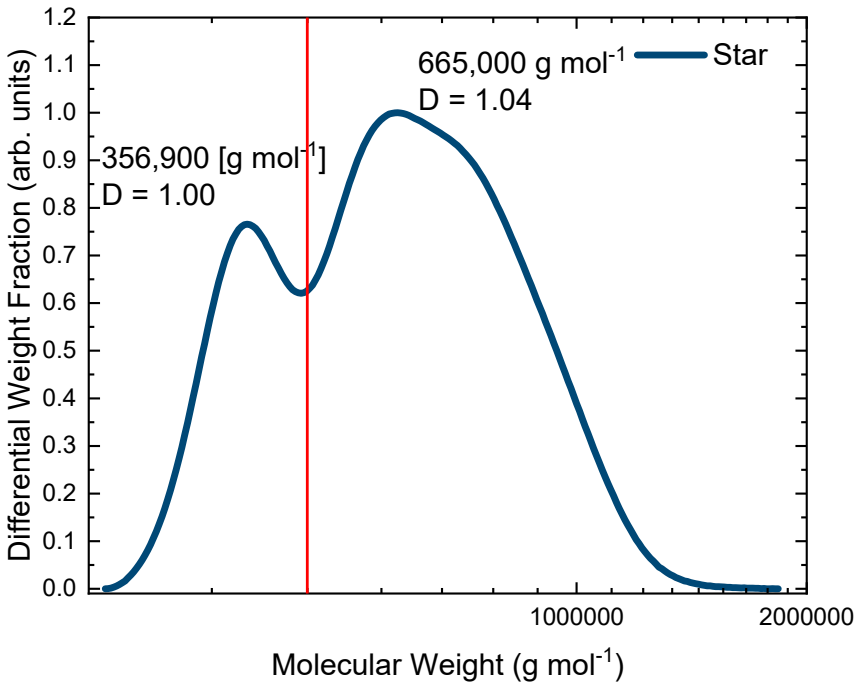

Figure S 1: Assumption of the composition of the final product as a bimodal distribution.

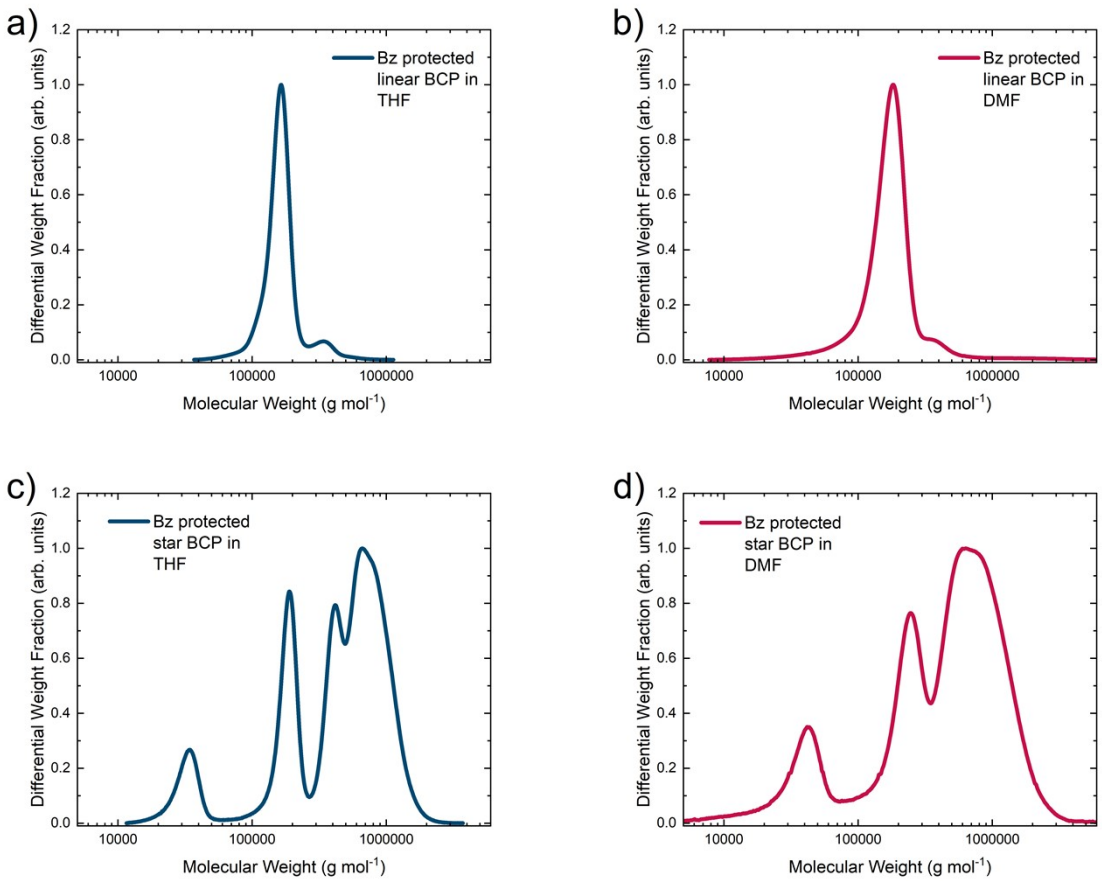

Figure S 2: Comparison of the SEC measurements in THF and DMF after protection using a Bz moiety for the linear BCP in THF (a), the linear BCP in DMF (b), the star-shaped BCP in THF (c), and the star-shaped BCP in DMF (d).

Table S 1: Compiled apparent molecular Weights (M_n) of the Bz-protected BCP with its dispersity given in brackets:

Bz-protected Polymer	in THF	in DMF
Linear	156,420 (1.11)	145,970 (1.40)
Star	624,680 (1.15)	457,650 (1.55)
Star (arm BCP)	181,440 (1.02)	238,190 (1.02)
Star (first Block)	30,810 (1.05)	37,861 (1,06)

Table S 2: Composition of the first cast solution for membrane preparation on a smaller scale for condition optimization:

Compound	m / mg	wt-%
Solvent mix[a]	2000	83
Polymer	400	17
$CuCl_2$	4.7	0.2

a: THF/DMF/DOX: 2/1/1

Table S 3: Conditions for each membrane of the first batch:

	M1a	M1b	M1c
Grammage (g/m^2)	80	50	50
Rel. Humidity (%)	25	27	26
Temperature (°C)	25	25	25

Evap. Time (s)	10	22	16
Pore Size (nm)	36.8 ± 9.9	41.3 ± 9.9	36.8 ± 8.4

Table S 4: Composition of the second cast solution for membrane preparation on a larger scale:

Compound	m / mg	wt-%
Solvent mix[a]	4030	83
Polymer	800	17
$CuCl_2$	5	0,1

a: THF/DMF/DOX: 2/1/1

Table S 5: Compilation of parameters for the second batch of membranes:

	M2a	M2b
Grammage (g/m^2)	1.566	1.566
Rel. Humidity (%)	26	24
Temperature (°C)	26	26
Evap. Time (s)	16	16
Weight of the membrane (mg)	384	325

Table S 6: Composition of the second cast solution for membrane preparation on a larger scale:

Compound	m / mg	wt-%
Solvent mix[a]	4030	83
Polymer	800	17
$CuCl_2$	5	0,1

a: THF/DMF/DOX: 2/1/1

Table S 7: Compilation of parameters for the third batch of membranes:

	M3
Grammage (g/m^2)	1.558
Rel. Humidity (%)	46
Temperature (°C)	22,5
Evap. Time (s)	17
Weight of the membrane (mg)	485 mg

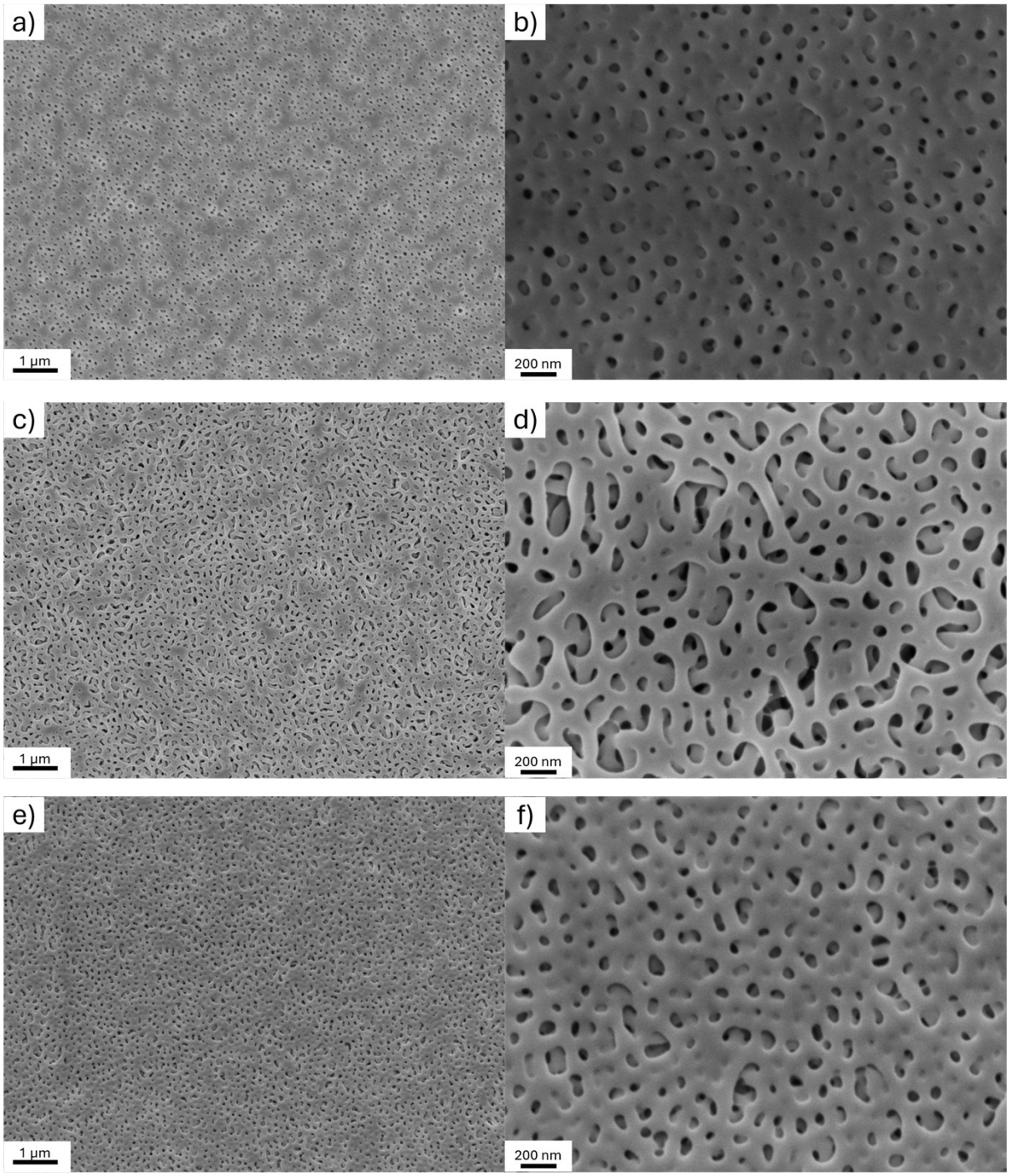

Figure S 3: Overview and detailed scanning electron micrographs of membranes M1a (a,b), M1b (c,d) and M1c (e,f).

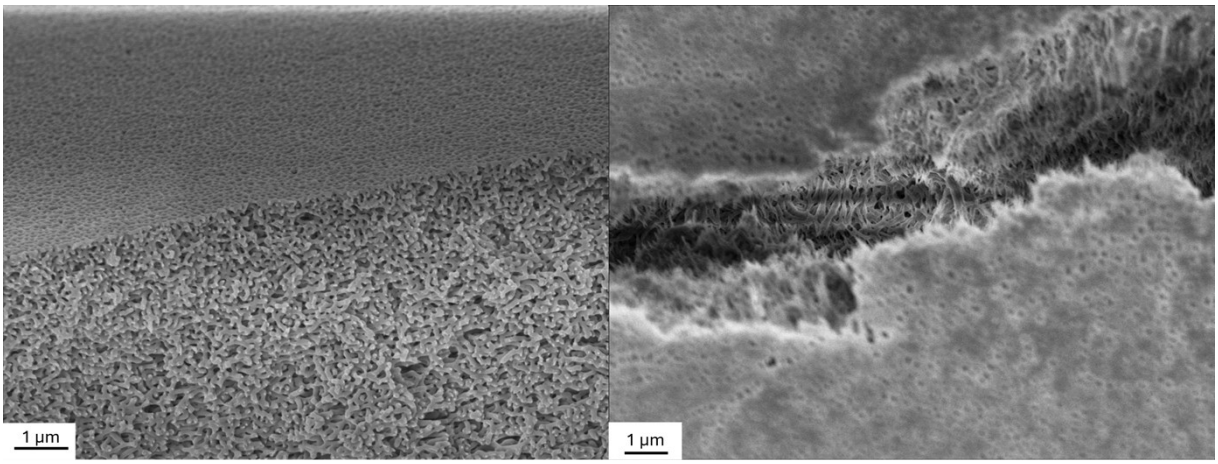

Figure S 4: Cross sections of M1a (left) and M1c (right).

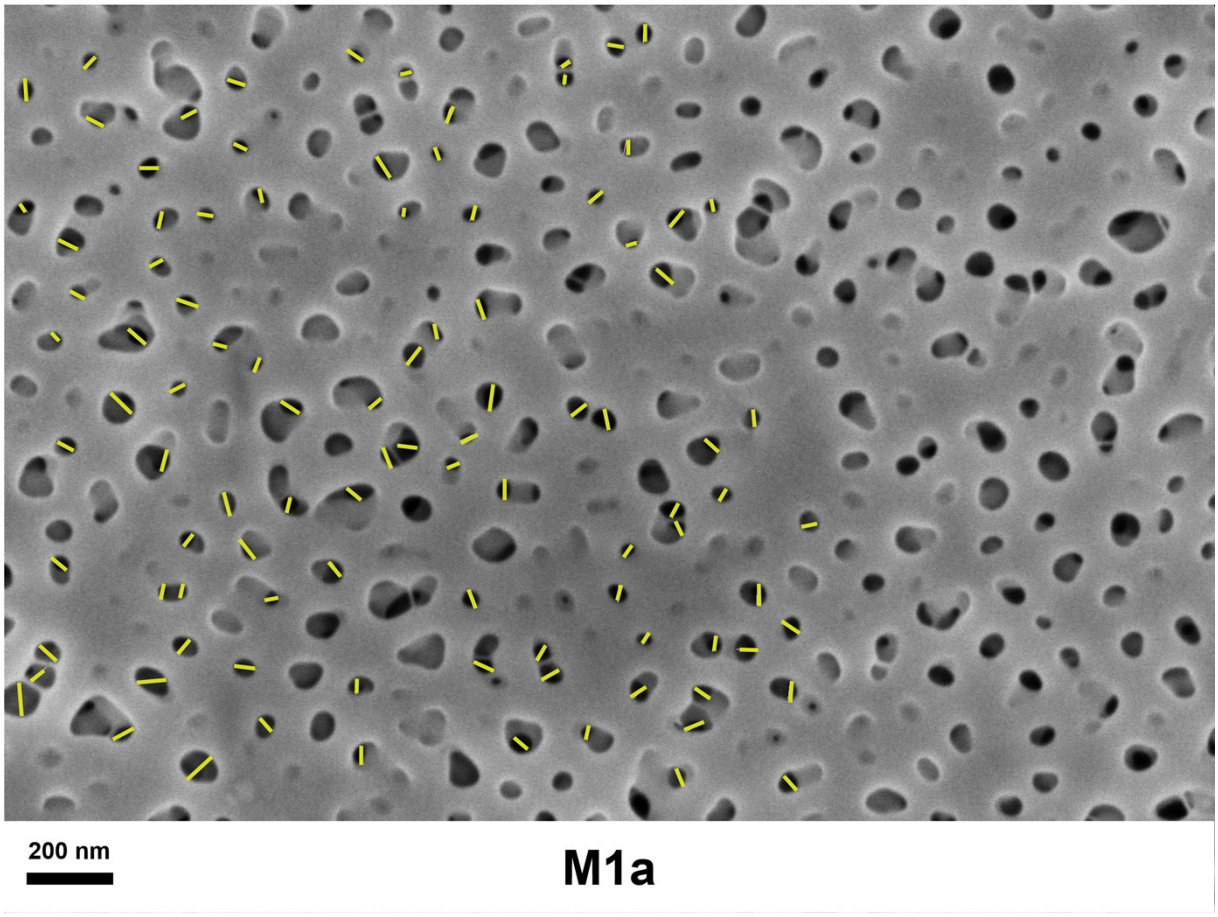

Figure S 5: Exemplary pore diameter measurements for M1 based on scanning electron micrographs. For pore-diameter determination, only defined and isolated pores were used.

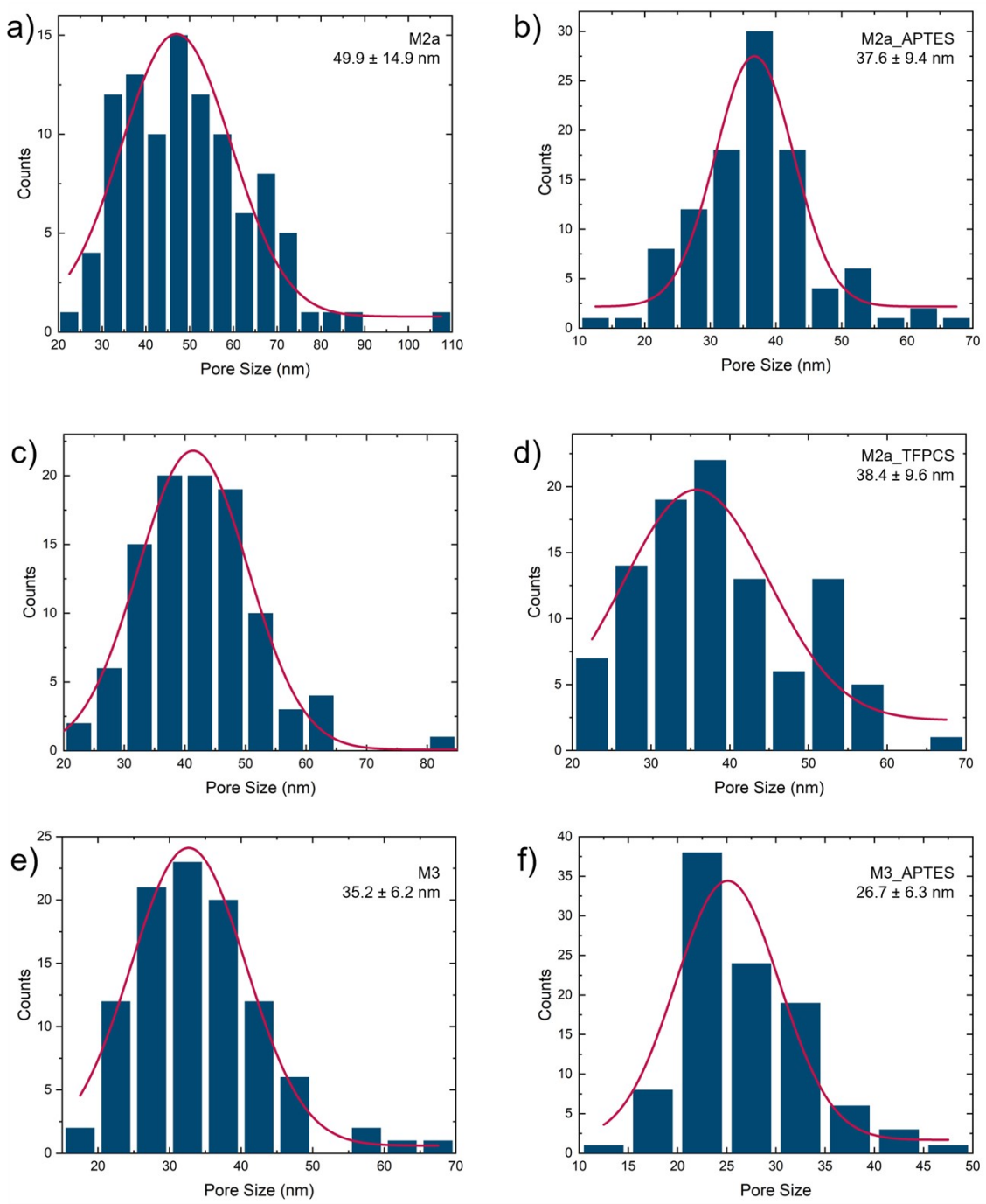

Figure S 6: Histograms for pore diameter determination for M2a (a), M2a_APTES (b), M2b (c), M2b_TFPCS, M3 (e), and M3_APTES (f).

Table S 8: Summary of recycle delays used for different samples (M2) and radical matrices. Note: These recycle delays d1 were calculated from the ^{1}H built-up times T_B obtained by ^{1}H saturation recovery experiment measured with microwave irradiation according to $d1=1.3 \cdot T_B$.

M2	Radical matrix	Recycle delay (s)
unmodified membrane	AMU	14
unmodified membrane	TEK	3
APTES-modified membrane	AMU	17
APTES-modified membrane	TEK	3
TFPCS-modified membrane	AMU	21
TFPCS-modified membrane	TEK	4

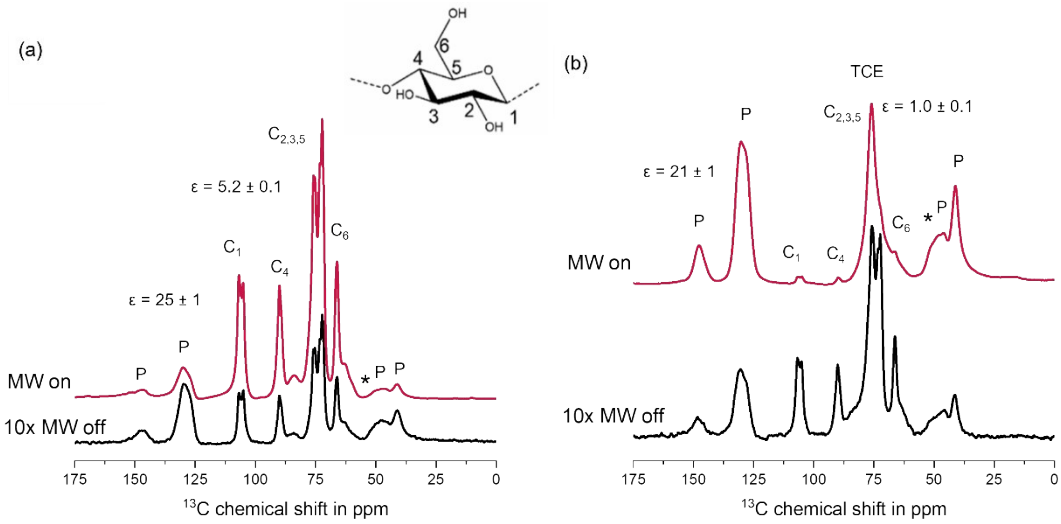

Figure S 7: 1H→13C CP MAS spectra of unmodified membrane (Linter Paper + PS-*b*-PDHPMA) measured with (MW On) and without (MW Off) microwave irradiation to visualize the sensitivity boost by DNP. For DNP NMR experiments, samples were prepared by impregnation with (a) a 15 mM AMUPol D2O/H2O (9:1) solution and (b) a 15 mM TEKPol in TCE solution. Spectra were recorded at 8 kHz spinning. Note: Spinning sidebands are marked with asterisks.

Dynamic nuclear polarization (DNP) enhancements strongly depend on the radical–solvent system. When using AMU as polarization matrix, enhancement factors of 25 ± 1 for PS-*b*-PDHPMA and 5.2 ± 0.1 for cellulose (BW-Linter) were obtained. In contrast, with TEK matrix enhancements of 21 ± 1 for PS-*b*-PDHPMA and only of 1.0 ± 0.1 for cellulose were obtained. These results indicate selective enhancement, with AMU favoring cellulose and TEK favoring PS-b-PDHPMA due to differences in radical accessibility and solvent–matrix interactions.

Table S 9: Summary of recycle delays used for different samples (M3) and radical matrices. Note: These recycle delays d1 were calculated from the ^{1}H built-up times T_B obtained by ^{1}H saturation recovery experiment measured with microwave irradiation according to $d1=1.3 \cdot T_B$.

M3	Radical matrix	Recycle delay (s)
unmodified membrane	AMU	8
unmodified membrane	TEK	4
APTES-modified membrane	AMU	12
APTES-modified membrane	TEK	3
TFPCS-modified membrane	AMU	12
TFPCS-modified membrane	TEK	3

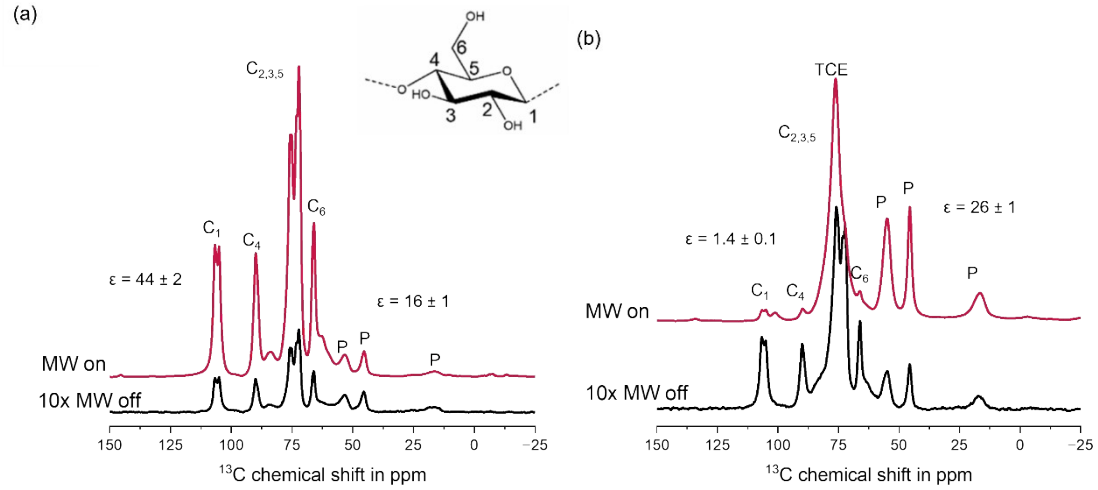

Figure S 8: 1H→13C CP MAS spectra of unmodified membrane (Linters Paper + PMMA-*b*-PDHPMA membrane) measured with (MW On) and without (MW Off) microwave irradiation to visualize the sensitivity boost by DNP. For DNP NMR experiments, samples were prepared by impregnation with (a) a 15 mM AMUPol D2O/H2O (9:1) solution and (b) a 15 mM TEKPol in TCE solution. Spectra were recorded at 8 kHz spinning. Note: Spinning sidebands are marked with asterisks.

Dynamic nuclear polarization (DNP) enhancements strongly depend on the radical–solvent system. When using AMU as polarization matrix, enhancement factors of 16 ± 1 for PMMA-*b*-PDHPMA and 44 ± 2 for cellulose (BW-Linter) were obtained. In contrast, with TEK matrix enhancements of 26 ± 1 for MMA/DHPMA and only of 1.4 ± 0.1 for cellulose were obtained. These results indicate selective enhancement, with AMU favoring cellulose and TEK favoring MMA/DHPMA due to differences in radical accessibility and solvent–matrix interactions.

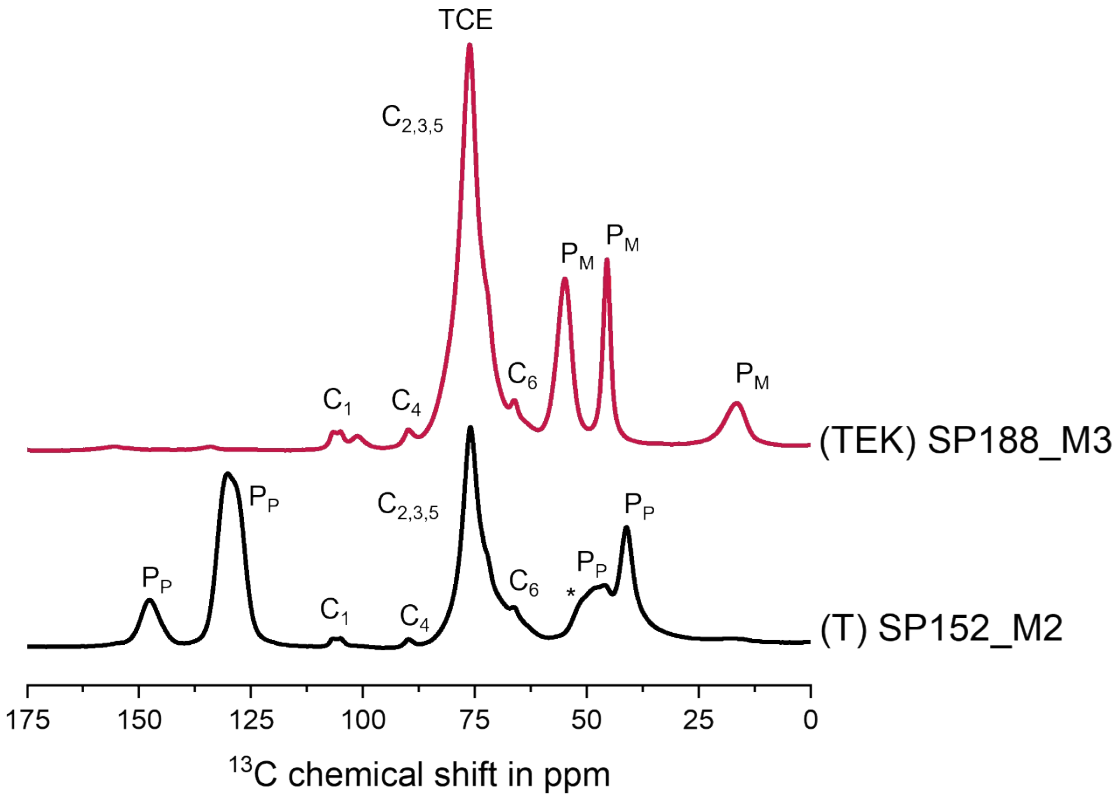

Figure S 9: DNP-enhanced 1H→13C CP MAS spectra of the unmodified membrane (BW-Linters 50 + PS-b-PDHPMA membrane) and unmodified membrane (BW-Linters 50 + MMA/DHPMA membrane) measured. Note: a 15 mM TEKPol in TCE (TEK) radical–solvent system was used for sample preparations. All spectra were recorded at 8 kHz spinning. Spinning sidebands are marked with an asterisk. Signals referring to the polymer are marked with "P".

Both membranes contain cellulose fibers as the structural backbone, clear differences are observed in the polymer-related carbon signals. For M2, the characteristic peaks of the PS-b-PDHPMA block copolymer appear at chemical shifts 42, 47, 130, and 148 ppm. In contrast, M3 exhibits a different set of polymer signals 16, 45, and 55 ppm, arising from the MMA/DHPMA block copolymer used in its preparation. These differences in peak positions directly reflect the distinct chemical structures of the polymers incorporated in each membrane. Importantly, because both spectra represent unmodified membranes, these polymer-related signals serve as the reference baseline for evaluating chemical changes after surface modification.